Sixth International Symposium on Turbulence and Shear Flow Phenomena
Seoul, Korea, 22-24 June 2009

CORE OF THE MAGNETIC OBSTACLE

E. V. Votyakov and S. C. Kassinos

Computational Science Laboratory UCY-CompSci
Department of Mechanical and Manufacturing Engineering,
University of Cyprus,
75 Kallipoleos, Nicosia 1678, Cyprus
votyakov@ucy.ac.cy, kassinos@ucy.ac.cy

ABSTRACT

Different recirculation patterns have been recently discovered in the electrically conducting flow around a magnetic obstacle, Votyakov et al. (2007, 2008). This paper continues the study and sheds new light on the core of the magnetic obstacle that develops between magnetic poles when the interaction parameter N, which is a ratio of Lorentz force to the inertial force, is very large. The core of the magnetic obstacle is streamlined both by the upstream flow and by the induced cross stream electric currents, like a foreign insulated insertion placed inside the ordinary hydrodynamic flow. In the core, closed streamlines of the mass flow resemble contour lines of electric potential, while closed streamlines of the electric current resemble contour lines of pressure.

INTRODUCTION

A magnetic obstacle is a region in the flow of an electrically conducting fluid, e.g. liquid metal, where an external inhomogeneous magnetic field, $\mathbf{B}$, is applied as shown in Fig. 1*a*. The rigid obstacle, such as a circular cylinder, is impenetrable for a flow since it represents a foreign solid insertion. The region of the magnetic obstacle manifests itself through the braking Lorentz force, $\mathbf{F_L} = \mathbf{j} \times \mathbf{B}$, originating from the interaction of $\mathbf{B}$ with electrical currents $\mathbf{j}$. The electrical currents are induced because of the electromotive force arising when the conducting liquid moves through the region of magnetic field.

Characteristics of the flow influenced by a magnetic obstacle are of considerable fundamental and practical interest. On the fundamental side, such a system possesses a rich variety of dynamical states, Votyakov et al. (2007). On the practical side, spatially localized magnetic fields enjoy a variety of industrial applications in metallurgy, e.g. Davidson (1999), including stirring of melts by a moving magnetic obstacle (called electromagnetic stirring), removing undesired turbulent fluctuations during steel casting using steady magnetic obstacles (called electromagnetic brake) and noncontact flow measurement using a magnetic obstacle (called Lorentz force velocimetry, e.g. Thess et al. (2006)). It is important to understand, for instance, whether the useful turbulence-damping effect of a magnetic brake is not obliterated by excessive vorticity generation in the wake of the magnetic obstacle.

New results about the wake of a magnetic obstacle have been reported recently by Votyakov et al. (2007, 2008). It has been found that a liquid metal flow subject to a local magnetic field shows different recirculation patterns: (1) no vortices, when viscous force prevails at small Lorentz force, (2) one pair of *inner magnetic* vortices between the magnetic poles, when Lorentz force is high and inertia small, and (3) three pairs, namely, magnetic as above, *connecting* and *attached* vortices, when Lorentz and inertial forces are high. The latter six-vortex ensemble is shown in Fig. 1*b*.

The goal of the current presentation is to study effects appearing in the laminar flow around the magnetic obstacle when the interaction parameter N, which is a ratio of Lorentz force to the inertial force, increases. When N is very large, both mass transfer and electric field vanish in the region between magnetic poles. This region, hereinafter called the core of the magnetic obstacle, looks as if frozen by the external magnetic field so that the upstream flow and crosswise electric currents can not penetrate inside it. Thus, the core of the magnetic obstacle is similar to a solid insulated obstacle inside an ordinary hydrodynamical flow with crosswise electric currents and *without* an external magnetic field. (This concerns hydrodynamics because there is no magnetic field, and the crosswise electric currents go around the insulated insertion without changing the mass flow.) Magnetic vortices are located aside the core and compensate shear stresses like a ball-bearing between the impenetrable region and upstream flow.

The presented results are new and complementary to those published in Votyakov et al. (2007, 2008). They required extensive sets of 3D numerical simulations: a series of runs for large N to refine the core of the magnetic obstacle.

It is worth to notice that our results for the core of a magnetic obstacle can be qualitatively understood from Kulikovskii's theory (Kulikovskii, 1968). In particular, mass flow (electric charge) streamlines resemble contour lines of the electric potential (pressure) in accordance to the main idea of Kulikovskii (1968). Nevertheless, to obtain quantitatively closed streamlines proper boundary conditions are necessary. They are obtained usually by integration along transverse magnetic field lines. This method works well for slowly varying magnetic fields, e.g. fringing fields (Alboussiere, 2004) because the Hartmann layers can be correctly imposed at the crossing of the field lines with channel walls. However, it is an open issue whether such an approach is valid in the case of a magnetic obstacle.

MODEL, EQUATIONS, NUMERICAL METHOD

The governing equations for electrically conducting and incompressible fluid are derived from the Navier-Stokes equation coupled with the Maxwell equations for moving medium and Ohm's law. By assuming that an induced magnetic field is infinitely small in comparison to the external

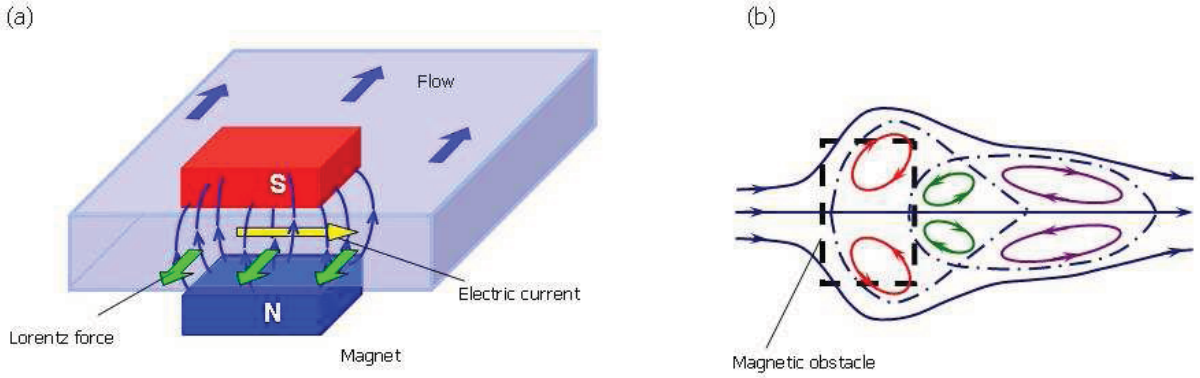

Figure 1: *a* - scheme of the magnetic obstacle created by two permanent magnets which are located on the top and bottom of the channel where an electrically conducting liquid flows. *b* - structure of the wake of the magnetic obstacle consisting of inner magnetic (first pair), connecting (second) and attached vortices (third pair). Dashed bold lines on *b* mark borders of the magnets.

magnetic field, the equations in dimensionless form are:

$$\frac{\partial \mathbf{u}}{\partial t} + (\mathbf{u}\cdot\nabla)\mathbf{u} = -\nabla p + \frac{1}{Re}\triangle\mathbf{u} + N(\mathbf{j}\times\mathbf{B}), \quad (1)$$

$$\mathbf{j} = -\nabla\phi + \mathbf{u}\times\mathbf{B}, \quad (2)$$

$$\nabla\cdot\mathbf{j} = 0, \quad (3)$$

$$\nabla\cdot\mathbf{u} = 0, \quad (4)$$

where $\mathbf{u}$ is velocity field, $\mathbf{B}$ is an external magnetic field, $\mathbf{j}$ is electric current density, p is pressure, ϕ is electric potential. The Reynolds number, $Re = u_0 H/\nu$, expresses a ratio between the inertia force and the viscous force and the interaction parameter, $N = B_0^2 H\sigma/(u_0\rho)$, expresses a ratio between the Lorentz force and the inertia force. Re and N are linked with each other by means of the Hartmann number: $Re\,N = Ha^2$, $Ha = HB_0(\sigma/\rho\nu)^{1/2}$ which determines the thickness δ of Hartmann boundary layers, $\delta/H \sim Ha^{-1}$, formed near the walls perpendicular to the direction of the magnetic field in the flow under constant magnetic field. Here, H is the characteristic length (size), u_0 is the characteristic flow velocity, B_0 the characteristic magnitude of the magnetic field intensity, ν is the kinematic viscosity of the fluid, σ is the electric conductivity of the fluid, and ρ is its density.

At given Re, N and $\mathbf{B}(x,y,z)$ the system of the partial differential equations shown above is solved in a 3D computational domain to obtain the unknown $\mathbf{u}(x,y,z)$, $p(x,y,z)$ and $\phi(x,y,z)$. The computational domain has periodical boundary conditions in the spanwise direction, and no-slip and insulating top and bottom walls in the transverse direction. The electric potential at the inlet and outlet borders is taken equal to zero. For the velocity, the outlet boundary is force free, and a laminar parabolic velocity profile is imposed at the inlet boundary. We are interested in a stationary laminar solution, hence, the initial conditions play no role.

The origin of the right-handed coordinate system, $x = y = z = 0$, is taken in the center of the magnetic gap. The size of the computational domain is: $-L_x \le x \le L_x$, $-L_y \le y \le L_y$, $-H \le z \le H$, where $L_x = 25$, $L_y = 25$, $H = 1$ and x, y, z are respectively the streamwise, crosswise, and transverse directions.

The characteristic dimensions for the Reynolds number Re, and the interaction parameter N are the half-height of the duct H, the mean flow rate u_0, and the magnetic field intensity B_0 taken at the center of the magnetic gap, $x = y = z = 0$. The range of the studied parameters is: $Re = 0.1, 1, 10, 100$ and $0 \ge N \ge 1000$.

The external magnetic field is modelled as a field from two permanent magnets occupying a space $\Omega = \{|x| \le M_x, |y| \le M_y, |z| \ge h\}$, where $M_x = 1.5$ ($M_y = 2$) is the streamwise (spanwise) width of the magnet, and $2\times h$ is the distance between magnetic poles. The magnets are supposed to be composed of magnetic dipoles oriented along the z-direction, therefore the total magnetic field $\mathbf{B}(x,y,z) = \nabla\int_\Omega \mathbf{B_d}(\mathbf{r},\mathbf{r'})d\mathbf{r'}$, where $\mathbf{B_d}(\mathbf{r},\mathbf{r'}) = \partial_{z'}(1/|\mathbf{r}-\mathbf{r'}|)$ is a field, at the point $\mathbf{r} = (x,y,z)$ created by the single magnetic dipole located in the point $\mathbf{r'} = (x',y',z')$. The integration can be performed analytically, see Votyakov et al. (2008), and after cumbersome algebraic calculations one obtains:

$$B_x(\mathbf{r}) = \frac{1}{B_0}\sum_{k=\pm1}\sum_{j=\pm1}\sum_{i=\pm1}(ijk)\,\mathrm{arctanh}\left[\frac{\delta_j}{\delta_{ijk}}\right],$$

$$B_y(\mathbf{r}) = \frac{1}{B_0}\sum_{k=\pm1}\sum_{j=\pm1}\sum_{i=\pm1}(ijk)\,\mathrm{arctanh}\left[\frac{\delta_i}{\delta_{ijk}}\right],$$

$$B_z(\mathbf{r}) = -\frac{1}{B_0}\sum_{k=\pm1}\sum_{j=\pm1}\sum_{i=\pm1}(ijk)\mathrm{arctan}\left[\frac{\delta_i\delta_j}{\delta_k\delta_{ijk}}\right],$$

where $\delta_i = (x - iM_x)$, $\delta_j = (y - jM_y)$, $\delta_k = (z - kh)$, and $\delta_{ijk} = [(x - iM_x)^2 + (y - jM_y)^2 + (z - kh)^2]^{1/2}$. The normalization factor B_0 is selected in such a way to have the intensity of the z-component equal one, $B_z(0,0,0) = 1$, in the center of the magnetic gap. Three-fold summation with the sign-alternating factor (ijk) reflects the fact that these equations are obtained by integrating over the 3D box Ω. Different cuts of the intensity $\mathbf{B}(\mathbf{r})$ are plotted in Fig. 3 and Fig. 4(*b*) in the paper of Votyakov et al. (2008).

The 3D numerical solver has been explained in details earlier, see Votyakov and Zienicke (2007). It was developed from a free hydrodynamic solver created originally in the research group of Prof. M. Griebel (Griebel et al. (1995)). The solver employs the Chorin-type projection algorithm and finite differences on an inhomogeneous staggered regular grid. Time integration is done by the explicit Adams-Bashforth method that has second order accuracy. Convective and diffusive terms are implemented by means of the VONOS (variable-order non-oscillatory scheme) method. The 3D Poisson equations are solved for pressure and electric potential at each time step by using the bi-conjugate gradient stabilized method (BiCGStab).

The numerical grid was regular and inhomogeneous, $N_x \times N_y \times N_z = 64^3$. The minimal horizontal step size in

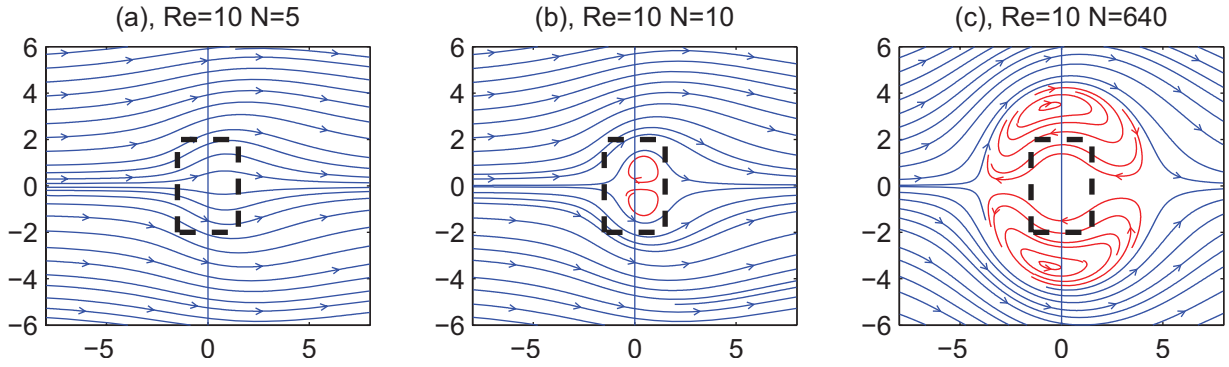

Figure 2: Streamlines in the central plane, $Re = 10$, N =5(a), 10(b), 640(c). Dashed bold lines mark borders of the magnets. As N gives rise, magnetic vortices move away each other by forming in between a core of the magnetic obstacle.

the region of the magnetic gap was $\Delta x \simeq \Delta y \simeq 0.3$, which means that a few dozens points were used for resolving the inner vortices in the core of the magnetic obstacle. The minimal vertical step size near the top and bottom (Hartmann) walls was $\Delta z = 0.005$. This corresponds to using three to five $(= (1/Ha)/\Delta z)$ points to resolve Hartmann layer at $Ha = 40 - 70$.

RESULTS

The goal of the simulations is to focus on the flow around a magnetic obstacle at large interaction parameter N. In order to achieve large $N = Ha^2/Re$, the simulations were started at a small interaction parameter and Ha was smoothly increased, while keeping Re constant. Several values of the Reynolds number were studied, $Re = 0.1, 1, 10, 100$, and no principal differences were found at the same N. These low values of Re imply low inertial forces, therefore, only two-vortex patterns were produced, without connecting and attached vortices.

The natural way to visualize the core of the magnetic obstacle is to plot streamlines of the flow in the central horizontal plane as shown in Fig. 2 at different interaction parameters N. Because N is the ratio of the Lorentz force to the inertial force, the larger N is, the stronger the retarding effect of the Lorenz force becomes. So, one observes no vortices at $N = 5$, Fig. 2a; the appearance of weak circular magnetic vortices at slightly below $N = 10$, Fig. 2b; and finally these vortices are well developed and strongly deformed at very large $N = 640$, Fig. 2c. In the latter case, the vortex streamlines envelop the bold dashed rectangle. This rectangle denotes the borders of the external magnet; inside the rectangle at large N one can see an island – a core of the magnetic obstacle. The observed deformation of the vortices and their drift from the center of the magnetic gap are due to the tendency of the flow to reduce its friction caused by retarding Lorentz force. The vortices are cambered and located in the shear layer alongside the magnetic gap in such a way that their rotation looks like the rotation of a ball-bearing inside the wheel.

The quantitative analysis of the core was performed by crosswise cuts through the center of the magnetic gap at different arising magnetic interaction parameters N. These cuts are shown in Fig. 3a for the streamwise velocity $u_x(y)$ and in Fig. 3b for the electric potential $\phi(y)$. First, we discuss how the streamwise velocity changes as N increases.

As shown in the Fig. 3a (curve 1), for the small $N = 0.1$, the velocity profile is only slightly disturbed with respect to a constant. As N increases, the curves $u_x(y)$ pull further down in the central part $u_{center} \equiv u_x(0)$, see for example curves 2 and 3. At N higher than a critical value $N_{c,m}$, i.e. for curve 4, the central velocities u_{center} are negative. This means that there appears a reverse flow causing magnetic vortices in the magnetic gap. When N rises even more (see curves 5 and 6) the magnetic vortices become stronger and simultaneously shift away from the center to the side along the y direction, see insertion in Fig. 3a for curves 5 and 6.

Fig. 3(b) shows how the electric potential $\phi(y)$ varies along the central crosswise cut through the magnetic gap. The slope in the central point is the crosswise electric field, $E_{y,center} = -d\phi/dy|_{y=0}$. One can see that $E_{y,center}$ changes its sign: it is positive at small N and negative at high N. To explain why it is so, one can use the following way of thinking. Any free flow tends to pass over an obstacle in such a way so as to perform the lowest possible mechanical work, i.e. flow streamlines are the lines of least resistance to the transfer of mass. The resistance of the flow subject to an external magnetic field is caused by the retarding Lorentz force $F_x \approx j_y B_z$, so the flow tends to produce a crosswise electric current, j_y, as low as possible while preserving the divergence-free condition $\nabla \cdot \mathbf{j} = 0$. To satisfy the latter requirement, an electric field $\mathbf{E}$ must appear, which is directed in such a way, so as to compensate the currents produced by the electromotive force $\mathbf{u} \times \mathbf{B}$. Next, we analyze the crosswise electric current $j_y = E_y + (u_z B_x - u_x B_z)$. Due to symmetry in the center of the magnetic gap $B_y = B_x = u_y = u_z = j_y = j_z = 0$ so $j_y = E_y - u_x B_z$. This means that E_y tends to have the same sign as u_x in order to make j_y smaller. At small N, the streamwise velocity u_x is large and positive, so the electric field E_y is positive too. When the magnetic vortices appear, there is a reverse flow in the center. Therefore, the central velocity is negative now, and the central electric field $E_{y,center}$ is also negative.

The change of the electric field in the magnetic gap can be explained in terms of the Poisson equation and the concurrence between external and internal vorticity, see Votyakov et al. (2008). Those arguments are also valid here, however in contrast to the previous study we have no side walls now, so the external vorticity in the present case plays only a minor role. As a result, the reversal of the electric field appears at a small N (approximately equal to five), which is close to $\kappa = 0.4$ given in Votyakov et al. (2008).

The overall data about u_{center} and $E_{y,center}$ in the whole range of studied N are shown in Fig. 4. One can see that both characteristics start from positive values, then, they cross the zeroth level, reach a minimum, go up again, and finally vanish in the limit of high N. With respect to

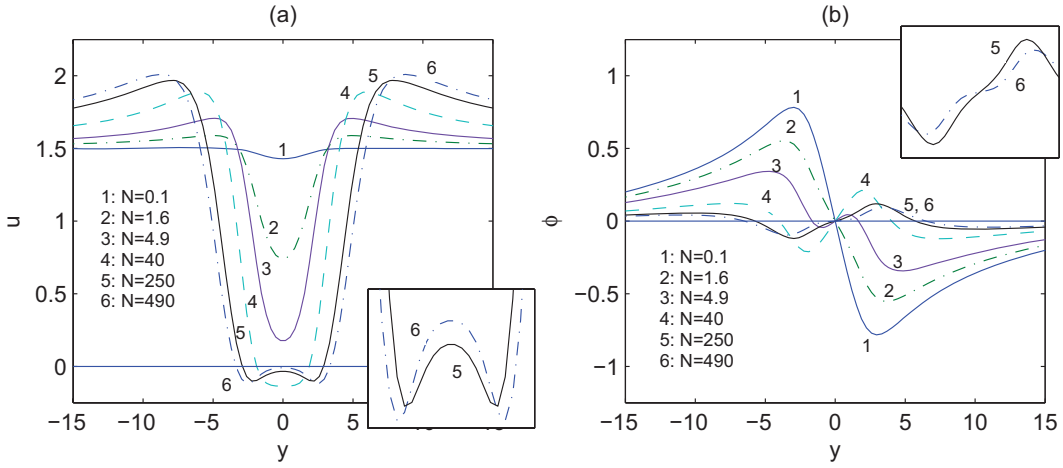

Figure 3: Streamwise velocity (a) and electric potential (b) along crosswise cuts of middle horizontal plane $x = z = 0$. $Re = 10$, N =0.1(solid 1), 1.6(dot-dashed 2), 4.9(solid 3), 40(dashed 4), 250(solid 5), and 490(dot-dashed 6). Insertion shows magnified plots for curves 5 and 6.

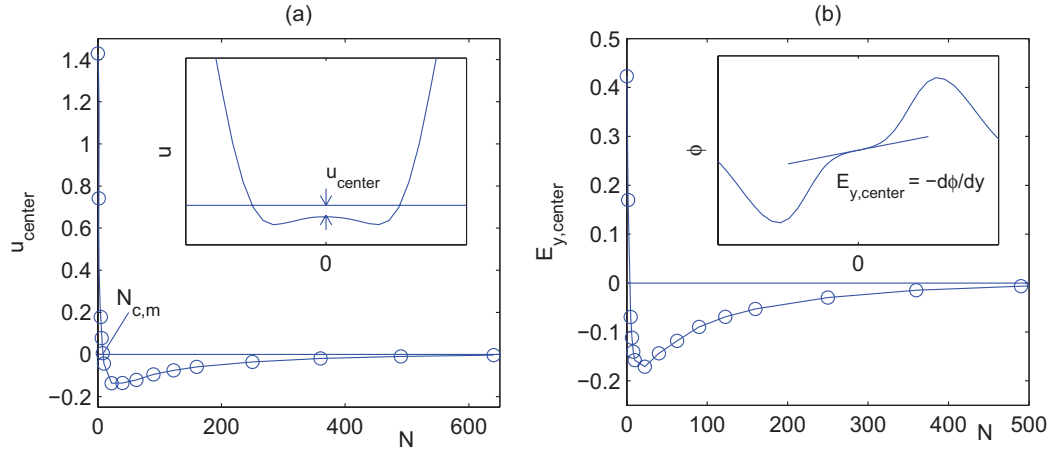

Figure 4: Central streamwise velocity u_{center} (a) and central spanwise electric field $E_{y,center}$ (b) as a function of the interaction parameter N. $N_{c,m}$ is a critical value where the streamwise velocity is equal to zero. Insertion shows the definition of u_{center} and $E_{y,center}$.

the streamwise velocity, this means that, at hight N, there is no mass flow in the center of the magnetic gap; the other velocity components are equal to zero due to symmetry. With respect to the crosswise electric field, this means that there are no electric currents. This occurs because there is no mass flow, therefore, the electromotive force vanishes, E_y goes to zero, and the other electric field components are equal to zero due to symmetry. Thus, one can say that the center of the magnetic gap is frozen by the strong external magnetic field, so that both mass flow and electric currents tend to bypass the center. In other words, this means that a strong magnetic obstacle has a core, and such a core is like a solid insulated body, being impenetrable for the external mass and electric charge flow.

When the inertia and viscous forces are negligible compared to the Lorentz force and pressure gradients, then mass flow streamlines must be governed by the electric potential distribution while the trajectories of the induced electric current must be governed by pressure distribution. This is derived straightforwardly from equations (1 – 2). Because inertia and viscosity are vanishing, the equations (1 – 2) become in the core and nearest periphery of the magnetic obstacle:

$$\nabla p = \mathbf{j} \times \mathbf{B}, \quad \nabla \phi = -\mathbf{j} + \mathbf{u} \times \mathbf{B} \approx \mathbf{u} \times \mathbf{B}\,.$$

In the latter formula, $\mathbf{j} \ll \nabla\phi$ and $\mathbf{u} \times \mathbf{B}$ is the dominating term. In the core of the obstacle, $\mathbf{B} = (0, 0, B_z) \approx (0, 0, 1)$, hence, the pressure (electric potential) is a streamline function for the electric current (velocity). These relationships for the flow under the strong external magnetic field have been published earlier by Kulikovskii (1968). In particular, this led to the introduction of the concept of "characteristic surfaces" – surfaces of equal intensity of the external heterogenous magnetic field – and the conclusion that the mass flow envelops these characteristic surfaces. However, as far no graphical illustration of this fact including recirculation patterns in the core of the magnetic obstacle had been presented.

Now, such an illustration is shown in Fig. 5 where one can easily make sure that there are similar mass flow streamlines (plot a) and electric potential contour lines (plot c) as well as electric current pathes (plot b) and pressure contour lines

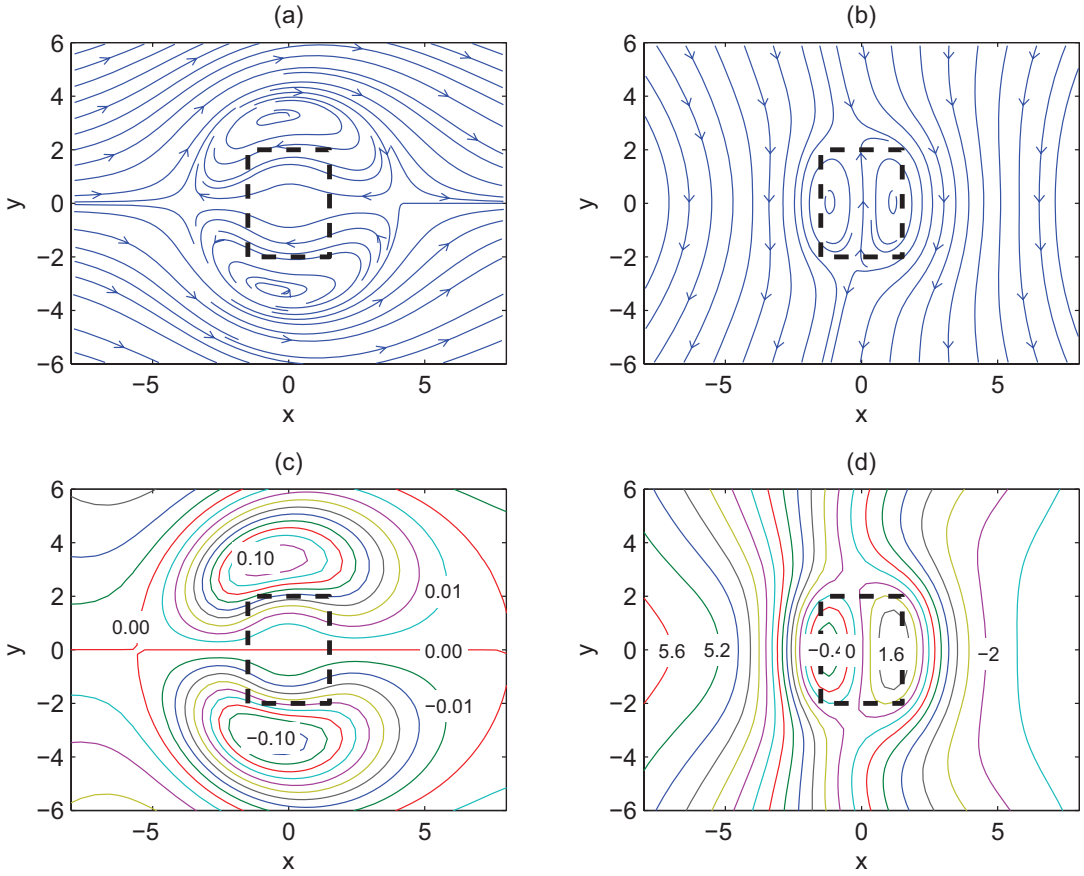

Figure 5: Middle horizontal plane, $z = 0$: streamlines of the mass (u_x, u_y) (a) and electric charge (j_x, y_y) (b) flow. Contour lines for the electric potential $\phi(x, y)$ (c) and pressure $p(x, y)$ (d) resemble the streamlines given above. $Re = 10$, $N = 490$. Contours of the electric potential are given with step 0.01, and contours of the pressure are given with the step 0.4. Dashed bold rectangle shows borders of the external magnet.

(plot d).

CONCLUSIONS.

For the first time, 3D numerical simulations are performed for a liquid metal flow subject to a strong external heterogenous magnetic field. The simulations shed light on the process of the formation of the core of the magnetic obstacle when the interaction parameter N is large. The core is surrounded by deformed magnetic vortices located in the shear layer. Inside the core there is no mass and electric transfer, i.e. at high N the magnetic obstacle is analogous to a solid hydrodynamical obstacle.

ACKNOWLEDGEMENTS

This work has been performed under the UCY-CompSci project, a Marie Curie Transfer of Knowledge (TOK-DEV) grant (Contract No. MTKD-CT-2004-014199). This work was also partially funded under a Center of Excellence grant from the Norwegian Research Council to the Center of Biomedical Computing.

REFERENCES

Alboussiere, T. 2004 A geostrophic-like model for large Hartmann number flows. *J. Fluid. Mech.* **521** 125–154.

Davidson, P. 1999 Magnetohydrodynamics in Materials Processing. *Annual Review of Fluid Mechanics* **31** 273–300.

Griebel, M., Dornseifer, T. and Neunhoeffer, T. 1995 *Numerische Strömungssimulation in der Strömungsmechanik*. Vieweg Verlag, Braunschweig.

Kulikovskii, A. 1968 Slow steady flows of a conducting fluid at high Hartmann numbers. *Izv. Akad. Nauk. SSSR Mekh. Zhidk. i Gaza* [No. 3] 3–10.

Thess, A., Votyakov, E. V. and Kolesnikov, Y. 2006 Lorentz Force Velocimetry. *Phys. Rev. Lett.* **96** 164501.

Votyakov, E. V., Kolesnikov, Y., Andreev, O., Zienicke, E. and Thess, A. 2007 Structure of the wake of a magnetic obstacle. *Phys. Rev. Lett.* **98** [No. 14] 144504.

Votyakov, E. V. and Zienicke, E. 2007 Numerical study of liquid metal flow in a rectangular duct under the influence of a heterogenous magnetic field. *Fluid Dynamics & Materials Processing* **3** [No. 2] 97–113.

Votyakov, E. V., Zienicke, E. and Kolesnikov, Y. 2008 Constrained flow around a magnetic obstacle. *J. Fluid. Mech.* **610** 131–156.